Neutron scattering studies of an antiferromagnetic Kondo compound: $Ce_8Pd_{24}Ga$

2001 J. Phys.: Condens. Matter 13 459

(http://iopscience.iop.org/0953-8984/13/3/308)

INSTITUTE OF PHYSICS PUBLISHING JOURNAL OF PHYSICS: CONDENSED MATTER

J. Phys.: Condens. Matter **13** (2001) 459–473 www.iop.org/Journals/cm PII: S0953-8984(01)08164-4

Neutron scattering studies of an antiferromagnetic Kondo compound: $Ce_8Pd_{24}Ga$

D T Adroja[1], B D Rainford[2], K S Knight[1] and P C Riedi[3]

[1] ISIS Facility, RAL, Chilton, Oxon OX11 OQX, UK
[2] Department of Physics, Southampton University, Southampton SO17 1BJ, UK
[3] School of Physics and Astronomy, St Andrews University, St Andrews KY16 9SS, UK

Received 27 September 2000, in final form 10 November 2000

Abstract

The antiferromagnet $Ce_8Pd_{24}Ga$ with $T_N = 3.1$ K has been investigated using neutron diffraction, inelastic neutron scattering, electrical resistivity, magnetoresistance and magnetic susceptibility measurements. Rietveld analysis of neutron diffraction data reveals that $Ce_8Pd_{24}Ga$ crystallizes in the cubic structure with space group $Pm\bar{3}m$. Inelastic neutron scattering (INS) studies show two well-defined crystal-field excitations at 3.2 meV and 12.8 meV. The crystal-field parameters have been estimated from the analysis of INS data. The heat capacity calculated from the crystal-field level scheme shows a Schottky peak at 15 K which agrees well with the reported experimental results. The resistivity exhibits $-\ln T$ behaviour at high temperature followed by a peak at 8 K and eventually drops at T_N. The peak in the resistivity at 8 K arises due to the combined effect of crystalline electric fields and Kondo interactions. The analysis of the resistivity data in the magnetically ordered state reveals a gap of 16.1 K in the spin-wave spectrum. At 1.8 K the magnetoresistance is positive and it changes to negative at 3 K. The positive magnetoresistance at 1.8 K is consistent with the antiferromagnetic ground state. The negative magnetoresistance shows a scaling behaviour that yields a low-temperature Kondo temperature of 5.8 K. The magnetic susceptibility exhibits Curie–Weiss behaviour between 20 K and 300 K with an effective paramagnetic moment $\mu_{eff} = 2.33\ \mu_B$ and paramagnetic Curie temperature $\theta_p = -18.8$ K. The present studies reveal that the physical properties of $Ce_8Pd_{24}Ga$ are governed by the Kondo, crystal-field and Ruderman–Kittel–Kasuya–Yosida (RKKY) interactions.

1. Introduction

Magnetic and transport studies of Ce-based intermetallics are of fundamental importance for the understanding of their unusual physical properties observed at low temperatures. The compounds of general formula CeX_3 (X = transition metal and metalloid atoms) occur in

several different structures, but those with X = In, Pd and Sn form in the cubic Cu_3Au-type structure [1–4]. Among these compounds, $CePd_3$ is a canonical intermediate-valence compound which has been extensively investigated using many experimental techniques [5–7]. The low-temperature properties of $CePd_3$ are consistent with a simple Fermi-liquid ground state, even though the carrier density is less than 0.3 electron per formula unit [8]. The transport properties reveal the onset of a coherent Kondo lattice ground state below 150 K [5].

In Kondo lattice compounds the existence of a magnetically ordered ground state depends on a balance between the indirect RKKY exchange interactions and on-site Kondo hybridization between the 4f electrons and the conduction electrons [9]. In the strong-hybridization limit, the so-called intermediate-valence state as found in $CePd_3$ and $CeSn_3$, the ground state is non-magnetic. For the limit of medium to weak hybridization, known as the heavy-fermion regime, there can be a variety of unusual ground states, including reduced-moment modulated antiferromagnetism, strange types of superconductivity and the Kondo insulating ground state. The hybridization strength is generally related to the number of holes in the s–p or d-like outer shells of a given ligand and to its distance from the Ce ions [10]. By decreasing the number of these holes we may dehybridize the 4f states, leading to a dramatic change in the magnetic and transport properties of the material. Such a dehybridization effect in $CePd_3$ has been observed when the compound is alloyed with an appropriate ligand or by introducing small atoms such as B, Si or Ge at the interstitial site in the Cu_3Au unit cell [11–14]. The interstitial impurities cause a dramatic crossover from archetypal intermediate-valence behaviour in $CePd_3$ to local moment character as seen through magnetic susceptibility and inelastic neutron scattering studies [11–14].

Recently, the crystal structure and magnetic properties of some of the $Ce_8Pd_{24}X$ (with X = Ga, In, Sn, Sb, Pb and Bi) compounds have been reported by Gordon *et al* and Cho *et al* [15–17]. These compounds are closely related to $CePd_3$ as $Ce_8Pd_{24}X$ may also be written as $CePd_3X_{0.125}$. A study of a $Ce_8Pd_{24}Sb$ single crystal using an x-ray four-circle diffractometer revealed that the crystal structure is composed of distorted perovskite and Cu_3Au subcells arranged with the perovskite-like units centred on the corners of the cube [15]. In the present work we have studied $Ce_8Pd_{24}Ga$ using neutron powder diffraction, inelastic neutron scattering, electrical resistivity, magnetoresistance and magnetic susceptibility measurements and the results of these studies are presented in this paper.

2. Experimental details

Polycrystalline samples of $Ce_8Pd_{24}Ga$ and $La_8Pd_{24}Ga$ were prepared by arc melting the stoichiometric amounts of the constituent elements with purity 99.9% on a water-cooled copper hearth under a high-purity argon atmosphere. The ingots were turned over and remelted several times to ensure homogeneity. X-ray powder diffraction studies with Cu Kα radiation were carried out to check the phase purity. Neutron powder diffraction measurements at room temperature were carried out using the HRPD diffractometer at the pulsed neutron source, ISIS Facility, Rutherford Appleton Laboratory, UK. Inelastic neutron scattering measurements were carried out using the time-of-flight spectrometer HET at ISIS with an incident neutron energy (E_i) of 40 meV. The energy resolution at zero energy transfer of the HET spectrometer is about 1.1 meV (FWHM) for $E_i = 40$ meV. The $Ce_8Pd_{24}Ga$ sample was cooled down to the lowest possible temperature of about 17 K in a closed-cycle refrigerator. Resistivity measurements were carried out using a standard four-probe dc technique between 1.3 K and 300 K. Magnetoresistance measurements were carried out using the standard four-probe dc technique and dc magnetic fields up to 12 T between 1.7 K and 30 K. Magnetic susceptibility measurements were carried out using a vibrating-sample magnetometer (VSM) between 3 K and 300 K.

3. Results and discussion

3.1. X-ray and neutron diffraction

X-ray powder diffraction studies reveal that the $Ce_8Pd_{24}Ga$ and $La_8Pd_{24}Ga$ samples were single-phase materials and crystallized in the cubic structure with lattice parameters $a = 8.3917(4)$ Å for $Ce_8Pd_{24}Ga$ and 8.4383(5) Å for $La_8Pd_{24}Ga$. The cubic lattice parameters of $Ce_8Pd_{24}Ga$ and $La_8Pd_{24}Ga$ are nearly double the lattice parameter, $a = 4.136$ Å, of $CePd_3$. This indicates the existence of a cubic supercell in $Ce_8Pd_{24}Ga$ and $La_8Pd_{24}Ga$. In order to further confirm the presence of the superlattice, we have carried out neutron powder diffraction measurements on $Ce_8Pd_{24}Ga$ at room temperature. A typical neutron diffraction pattern from the 168.3° bank of the HRPD diffractometer is shown in figure 1. The diffraction pattern shows that the sample is largely single phase but contains a small impurity phase. The impurity peaks (marked with crosses in figure 1) have intensities less than 0.5% of that of the main peak. The diffraction pattern of $Ce_8Pd_{24}Ga$ was refined using the TF12LS program available at ISIS and the same structural model, with space group $Pm\bar{3}m$ (No 221), as was proposed for $Ce_8Pd_{24}Sb$ [15]. In this space group, Ce atoms occupy the crystallographic 8g sites, Pd atoms occupy three different types of site, Pd1 at the 6f sites, Pd2 at the 6e sites and Pd3 at the 12h sites, and Sb atoms occupy the 1a sites.

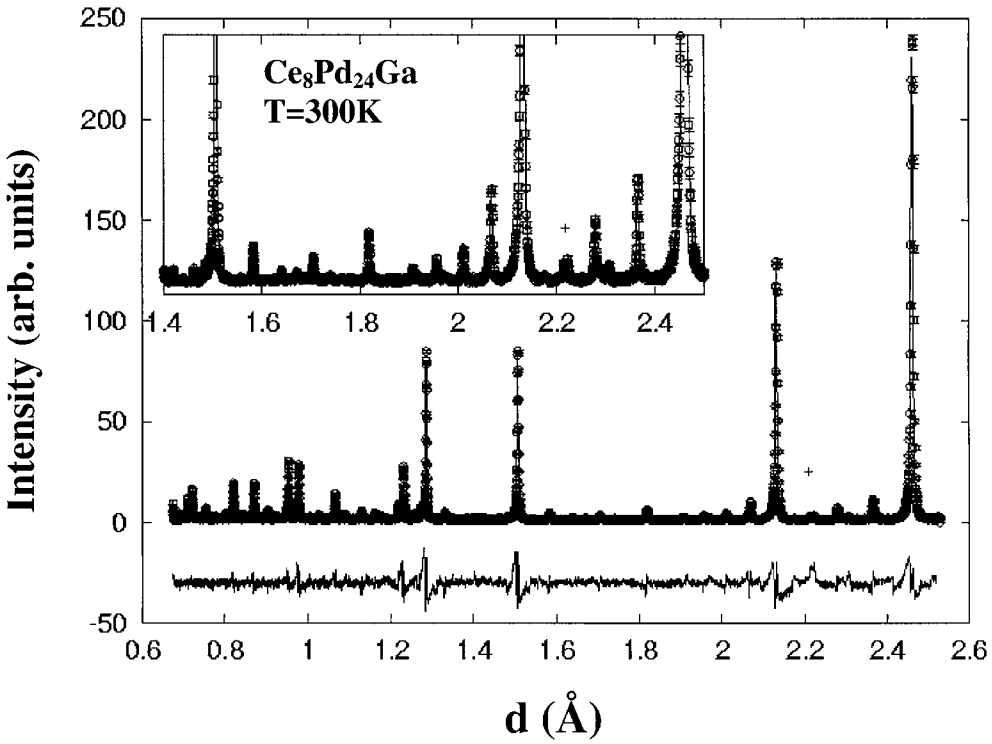

Figure 1. A typical room temperature neutron diffraction pattern of $Ce_8Pd_{24}Ga$ measured on the HRPD diffractometer at the ISIS facility. The experimental data are shown by the symbols, while the line through the data represents the results of the Rietveld refinement. The lower curve is the difference curve for the experimental data and the calculated curve. The inset shows the diffraction pattern for a limited d-range with an expanded y-axis. A plus symbol shows an impurity phase.

The refinement was carried out in four stages. In the first stage the background, lattice parameters and peak-shape parameters were varied, while in the second stage the atomic position parameters and isotropic temperature factors were refined. The site occupancies were varied in the third stage and all parameters were allowed to vary in the final stage. The parameters obtained from the last cycle of the refinement are given in table 1 and the results of the refinement are shown by solid lines in figure 1. The reduced χ^2 and the residuals, the profile R-factor (R_p), weighted profile R-factor (R_{wp}), expected R-factor (R_E) and intensity (or Bragg) R-factor (R_I), are also given in the same table and they are defined as in [18]:

$$\chi^2 = M/(N_{obs} - N_{var} + C) \tag{1}$$

$$R_p = \sum |Y_{obs} - Y_{calc}| \Big/ \sum Y_{obs} \tag{2}$$

$$R_{wp} = \left(M \Big/ \sum w Y_{obs}^2 \right)^{1/2} \tag{3}$$

$$R_E = \left[(N_{obs} - N_{var} + C) \Big/ \sum w Y_{obs}^2) \right]^{1/2} \tag{4}$$

$$R_I = \sum |I_{obs} - I_{calc}/C| \Big/ \sum I_{obs} \tag{5}$$

where

$$M = \sum w(Y_{obs} - Y_{calc})^2. \tag{6}$$

Here Y_{obs} (I_{obs}) and Y_{calc} (I_{calc}) are the measured and calculated profile (intensity), respectively, w is a weighting factor, N_{obs} and N_{var} are the number of data points and fitting parameters, respectively, and C is the number of constraints. The occupancy fractions show that the Ce and Pd sites are fully occupied, while the Ga site is 78% occupied. The crystal structure of $Ce_8Pd_{24}Ga$ is composed of distorted perovskite and Cu_3Au subcells as shown in figure 2. The large atomic size of the Ga atom pushes the Pd atoms out of the phases of the cubic cell and produces a distortion in the Cu_3Au cell. On the other hand a small atom like B occupies the body-centre interstitial site in $CePd_3$ without any distortion of the Cu_3Au unit cell. The interatomic distances calculated from the above parameters are given in table 2. The shortest bond distance is 2.453 Å for Ga and Pd2 compared to the sum of their covalent radii (2.54 Å). Such a small distance between these atoms indicates a strong overlap between p electrons of Ga and d electrons of Pd, which is responsible for the Ce 4f–Pd 4d dehybridization and hence the dramatic change in the magnetic and transport properties of $Ce_8Pd_{24}Ga$ compared to those of $CePd_3$.

Table 1. Atomic coordinates, site occupancies (S.O.) and isotropic displacement parameters U_{eq} (in pm^2) for $Ce_8Pd_{24}Ga$ obtained from the full-structure Rietveld refinement using the $Pm\bar{3}m$ space group. The S.O. of Ce1 was kept fixed.

Atom	Wyckoff site	x	y	z	S.O.	U_{eq}
Ce1	8g	0.2509(2)	0.2509(2)	0.2509(2)	1.00	22(9)
Pd1	6f	0.2544(3)	0.500	0.500	1.04(2)	64(8)
Pd2	6e	0.2923(3)	0.000	0.000	1.01(2)	96(11)
Pd3	12h	0.2599(2)	0.500	0.000	1.06(2)	84(7)
Ga1	1a	0.000	0.000	0.000	0.78(4)	58(29)
	Rietveld[a]	$\chi^2 = 6.71$	$R_p = 9.62\%$	$R_{wp} = 12.32\%$	$R_E = 4.76\%$	$R_I = 3.88\%$
	CAILS[b]	$\chi^2 = 6.27$	$R_p = 8.96\%$	$R_{wp} = 11.80\%$	$R_E = 4.71\%$	

[a] Full-structure Rietveld refinement.
[b] CAILS refinement, for comparison only.

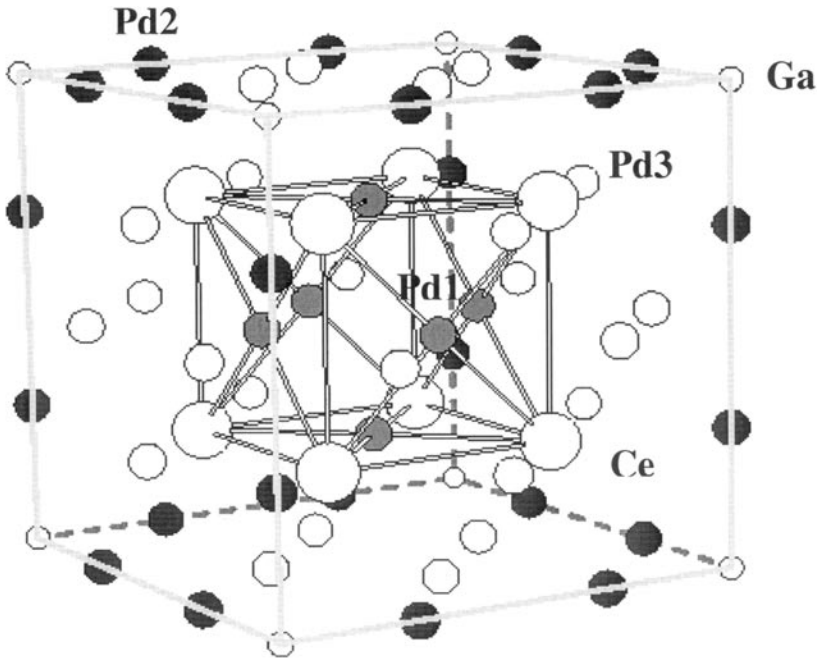

Figure 2. The crystal structure of $Ce_8Pd_{24}Ga$. The small-size circles represent Ga atoms, medium-size circles represent Pd (grey = Pd1, black = Pd2 and white = Pd3) atoms and large-size circles represent Ce atoms.

Table 2. Interatomic distances of $Ce_8Pd_{24}Ga$. All distances less than 4.5 Å are shown. The standard deviations are typically 0.001 Å or less.

Ce1:	3Pd1 2.957	Pd1:	4Pd1 2.915	Pd2:	1Ga1 2.453	Pd3:	2Pd2 2.792
	6Pd3 2.968		4Pd3 2.936		4Pd3 2.792		2Pd3 2.849
	3Pd2 2.999		4Ce1 2.957		4Ce1 2.999		2Pd1 2.936
	1Ga1 3.646		1Pd1 4.122		1Pd2 3.486		4Ce1 2.968
	3Ce1 4.181		4Pd3 4.196		4Pd2 3.469		2Pd3 3.085
	3Ce1 4.211		1Pd1 4.270		4Pd3 4.205		1Pd3 4.029
							2Pd1 4.196
							1Pd3 4.362
Ga1:	6Pd2 2.453						
	8Ce1 3.646						

It is to be noted that even though the quality of the fit is reasonably good (see figure 1), the observed values of the reduced χ^2 and residuals R_p and R_{wp} as well as R_E are high (see table 1). On the other hand, the value of $R_I = 3.88\%$ indicates that the structural model is correct. It is to be noted that R_I determines the quality of the structural fit since it is related to peak area and not peak shape. To discover the origin of the high values of χ^2, R_p, R_{wp} and R_E, we have also refined our neutron diffraction data on the basis of the CAILS–Pawley (cell and intensity least-squares) refinement method using the $Pm\bar{3}m$ space group. The CAILS refinement method is different from the traditional Rietveld refinement technique (used above) in that only cell parameters, peak-width parameters and integrated intensities are refined. CAILS refinement is independent of the atomic position parameters (or structural model) and only depends on

the space group symmetry. In this method the intensities of all peaks vary independently. The values of χ^2 and the R-factors obtained from the CAILS refinement are given in table 1. The values of χ^2, R_p, R_{wp} and R_E obtained from the CAILS refinement are also high and nearly the same as those obtained from the full-structure Rietveld refinement discussed above. This reveals that the high values of χ^2 and the R-factors are not due to an incorrect structural model. Further, detailed examination of the refined profile in both methods reveals that the observed peak shape is different from the peak shape calculated using the Voigt function convolved with a double-exponential decay and switch function (see the inset of figure 1 and the difference curve in figure 1). This explains the high values of χ^2, R_p, R_{wp} and R_E found by both methods. At present we do not understand why the observed peak shape is different from the calculated one. We also refined our data on the basis of rhombohedral symmetry, space group $R\bar{3}m$ (No 166), and the Rietveld refinement method. However, the values of the R-factors obtained using the $R\bar{3}m$ space group were higher than those obtained using the $Pm\bar{3}m$ space group; hence we discard the possibility of the $R\bar{3}m$ space group being correct.

3.2. Inelastic neutron scattering

Figure 3(a) shows inelastic neutron scattering spectra of $Ce_8Pd_{24}Ga$ at 17 K measured on the HET spectrometer with incident neutron energy $E_i = 40$ meV: the symbols rerepresent the total response (magnetic plus phonon) averaged over a low-Q region (0.7–2.2 Å^{-1}) and the histogram is an estimate of the phonon response extrapolated from the high-Q region (7.8–8.2 Å^{-1}). The magnetic scattering is intense at low Q-values and negligible at high Q-values because of the magnetic form factor ($F(Q)$), while the phonon scattering is dominant at high Q-values and suppressed at the low Q-values: the magnetic scattering $\propto F(Q)^2$ which decreases with Q, while the phonon scattering $\propto Q^2$, which increases with Q. We have used the standard scaling method to subtract the phonon response from the measured total response at low Q, by using the measured phonon response at high Q. By subtracting the estimated phonon response from the total measured response at the low Q, we deduced the magnetic scattering in the low-Q spectrum, which is shown in figure 3(b). The magnetic response shows two well-defined crystal-field (CF) excitations at energies of 3.2 meV and 12.8 meV, corresponding to transitions from the ground-state doublet to the two excited CF doublets. It is noteworthy that the inelastic response of $CePd_3$ does not show any sign of CF excitations; instead it exhibits a broad peak centred at 65 meV with a linewidth of 68 meV [19, 20]. The point symmetry of the Ce ions in $Ce_8Pd_{24}Ga$ is $3m$, which is lower than cubic. This gives two additional terms in the cubic CF Hamiltonian of the Ce^{3+} ion with $J = 5/2$. We have verified this by direct calculation with the superposition-model approach [21], using a suitable choice of quantization axes. This showed the presence of one rank-2 and two rank-4 terms in the CF Hamiltonian:

$$H_{CF} = B_2^0 O_2^0 + B_4^0 O_4^0 + B_4^3 O_4^3 \tag{7}$$

where the B_n^m are the crystal-field parameters and the O_n^m are the Stevens operator equivalents [22]. H_{CF} has only three independent CF parameters; thus the positions and relative intensities of the two CF excitations are sufficient for estimating a unique set of CF parameters. The values of the CF parameters obtained from the least-squares fit to the INS data are (in meV) $B_2^0 = 0.551(5)$, $B_4^0 = 0.024(2)$ and $B_4^3 = 0.208(4)$. The solid line in figure 3(b) represents the fitted response, with this set of CF parameters, which agrees well with the observed magnetic response. The linewidth of the first excitation is 2.06(5) meV, while that of the second excitation is 1.63(4) meV. We would like to mention here that the quasielastic magnetic scattering around zero energy transfer in $Ce_8Pd_{24}Ga$ could not be determined due to the presence of strong elastic

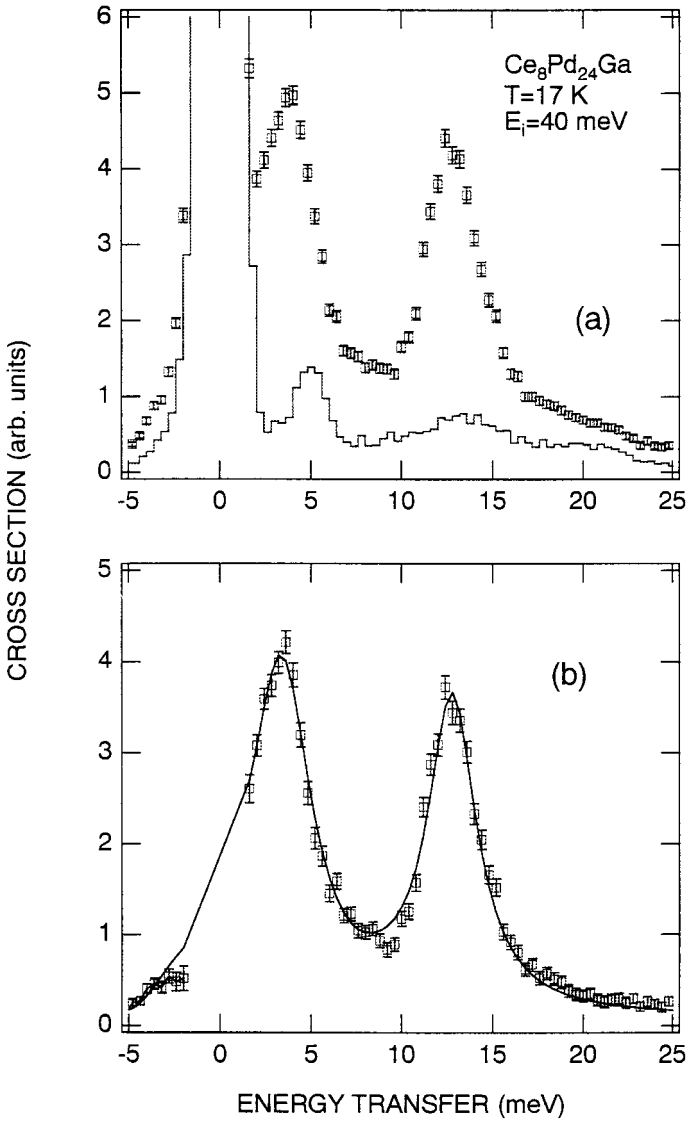

Figure 3. (a) The inelastic neutron scattering response from $Ce_8Pd_{24}Ga$ at 17 K measured on the HET spectrometer. The symbols show the experimental data summed over the scattering angles between 8° and 30°, while the histogram is an estimate of the phonon scattering extrapolated from the high-angle (132°) detector bank. (b) The magnetic response from $Ce_8Pd_{24}Ga$ at 17 K (symbols). The solid line represents the fit based on the crystal-field model (see the text).

scattering at high Q-values, which gave a negative contribution to the magnetic response around zero energy transfer.

Having obtained information about the crystal-field energy-level scheme of $Ce_8Pd_{24}Ga$, it would be interesting to calculate the heat capacity to help with understanding the reported high value of the electronic specific heat divided by the temperature (C_{el}/T; see figure 4(a) in reference [17]) between T_N and 16 K. Here we give a brief discussion of the heat capacity data from reference [17]. The value of the specific heat coefficient, γ_p, estimated at $T \rightarrow 0$

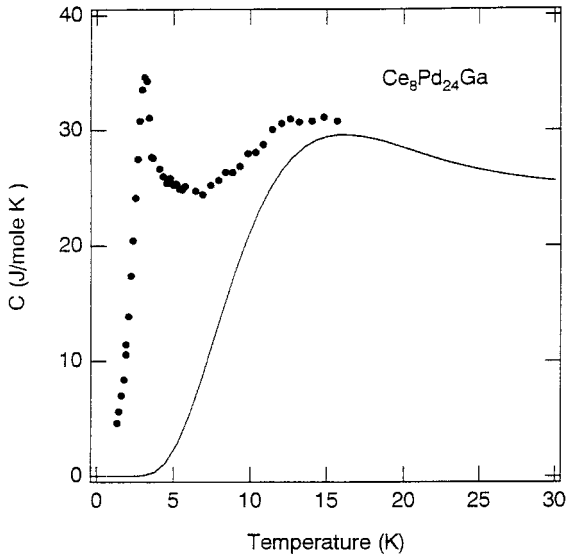

Figure 4. Heat capacity versus temperature for $Ce_8Pd_{24}Ga$; data from reference [17]. The solid line shows the heat capacity calculated on the basis of the crystal-field level scheme (see the text).

from extrapolating the linear behaviour of the C_{el}/T versus T^2 curve between 7 K and 16 K is 3.3 J mol^{-1} K^{-2} [17]. This value of γ_p is very high compared with the values of γ_p for $Ce_8Pd_{24}T$ (T = In, Sb, Bi, Sn, Pb) [17] and other Ce-based heavy-fermion systems. As reported in reference [17], the entropy change (ΔS) associated with the magnetic phase transition is 16.4 J mol^{-1} K^{-1}, which is smaller than $8R\ln(2) = 46.1$ J mol^{-1} K^{-1} (where R is the gas constant) expected from a doublet CF ground state. The small value of the estimated entropy was attributed to either itinerant electrons with heavy effective mass being partly involved in the phase transition or magnetic ordering of induced moment type. The calculated heat capacity results along with experimental data from reference [17] are shown in figure 4. The calculated heat capacity exhibits a Schottky peak at 15 K, in agreement with the experimental results. The reported high value of C_{el}/T in the paramagnetic state (i.e. between T_N and 16 K) therefore arises from the Schottky contribution to the heat capacity. This would also partly explain the high value of γ_p estimated from the linear behaviour of the heat capacity between 7 and 16 K.

3.3. Resistivity

Figure 5(a) shows the resistivity ρ versus temperature for $Ce_8Pd_{24}Ga$ and $La_8Pd_{24}Ga$ compounds. $\rho(T)$ for $La_8Pd_{24}Ga$ decreases almost linearly with decreasing temperature down to 1.3 K, indicating metallic behaviour. On the other hand, $\rho(T)$ for $Ce_8Pd_{24}Ga$ increases with decreasing temperature from 300 K, exhibits a broad maximum at 8 K and eventually drops below 3.3 K due to antiferromagnetic ordering of the Ce moments. In figure 5(b) we have plotted the temperature derivative of the resistivity, $\mathrm{d}\rho/\mathrm{d}T$, versus T (secondary y-axis). It is interesting to note that on reaching T_N, the divergence in $\mathrm{d}\rho/\mathrm{d}T$ is similar to that observed in the heat capacity (see figure 4). This type of similarity in the critical divergence between $\mathrm{d}\rho/\mathrm{d}T$ and the heat capacity has been shown theoretically for antiferromagnetic ordering by Kasuya and Kondo [23].

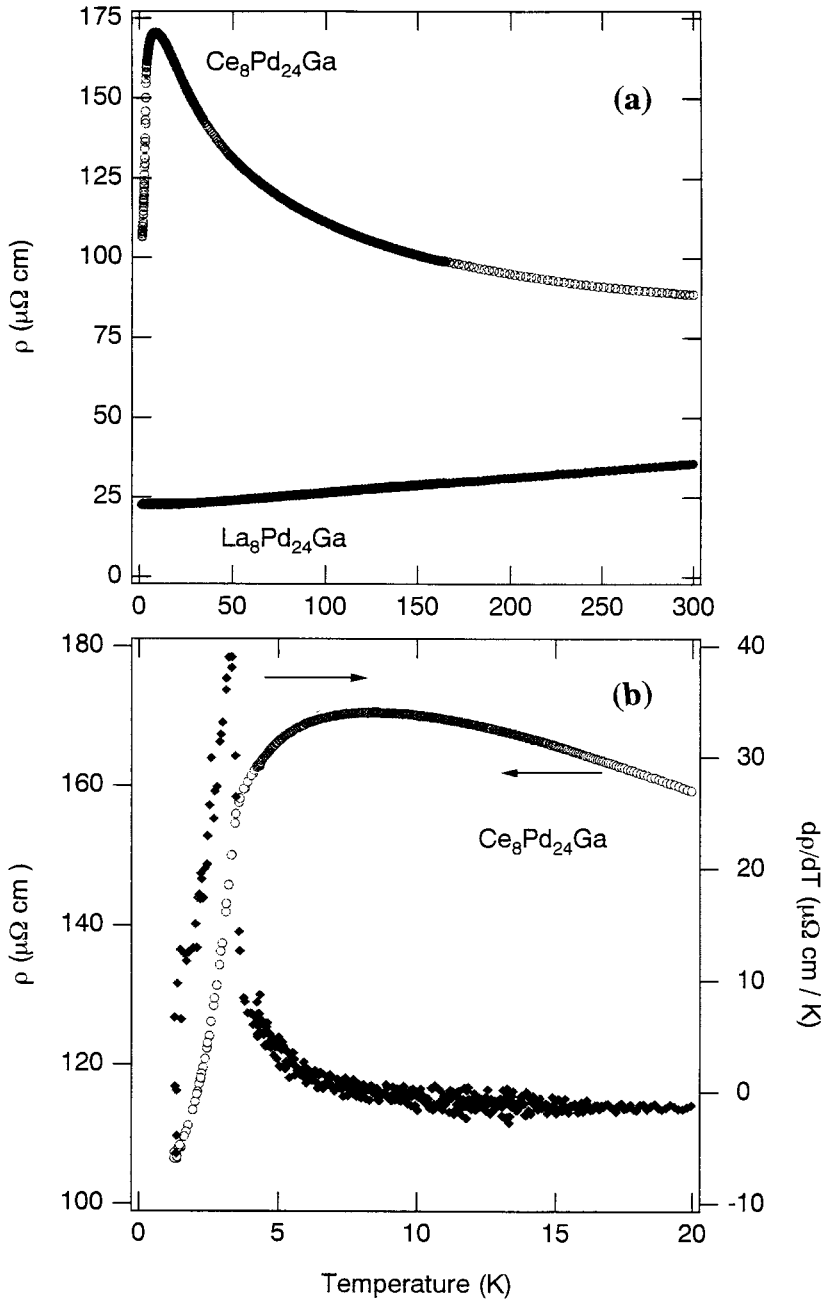

Figure 5. (a) Resistivity ρ versus temperature for $Ce_8Pd_{24}Ga$ and $La_8Pd_{24}Ga$ and (b) ρ versus T and the temperature dependence of $d\rho/dT$ for $Ce_8Pd_{24}Ga$ at low temperatures.

The magnetic contribution to the resistivity, ρ_m, of $Ce_8Pd_{24}Ga$ was estimated by subtracting the resistivity of $La_8Pd_{24}Ga$, which is plotted as ρ_m versus $\ln T$ in figure 6. In the high-temperature regime, ρ_m exhibits $-\ln T$ behaviour, followed by a maximum at 8 K. The $-\ln T$ behaviour is due to incoherent Kondo scattering of conduction electrons by the localized

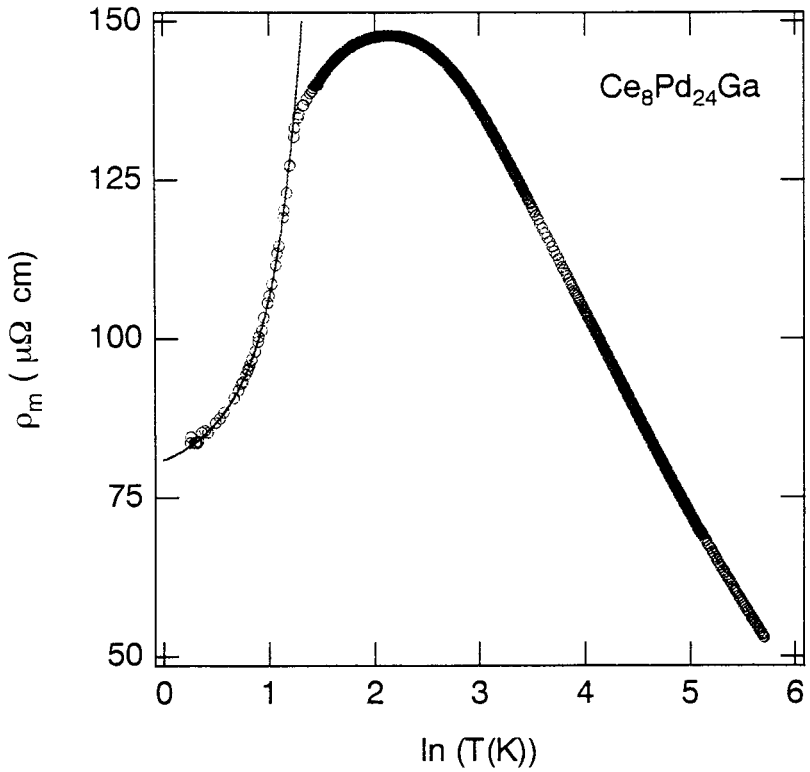

Figure 6. The magnetic part of the resistivity ρ_m versus ln T for $Ce_8Pd_{24}Ga$.

4f moments, while the maximum arises from the combined presence of Kondo and crystalline-electric-field effects. This type of resistivity behaviour has been explained theoretically by Cornut and Coqblin [24] and very recently by Fischer [25]. Below T_N, $\rho_m(T)$ behaviour is influenced by the presence of spin waves and can be described by

$$\rho_m(T) = \rho_0 + AT^2 + C(T/\Delta)(1 + 2T/\Delta)\exp(-\Delta/T) \tag{8}$$

where ρ_0 is the residual resistivity, AT^2 the normal Fermi-liquid contribution and Δ the gap in the spin-wave spectrum [26]. The values of the parameters obtained from the least-squares fit to the $\rho_m(T)$ data below T_N are: $\rho_0 = 77.6(\pm 0.1)$ $\mu\Omega$ cm, $A = 3.45(\pm 0.02)$ $\mu\Omega$ cm K^{-2}, $C = 5510(\pm 150)$ $\mu\Omega$ cm and $\Delta = 16.1(\pm 0.1)$ K. The fit to the resistivity data is shown by the solid line in figure 6. The value of A is higher than the value 0.072 $\mu\Omega$ cm K^{-2} observed for $CePd_3$ [27]. The high value of A for $Ce_8Pd_{24}Ga$ is consistent with the observed high value of γ, as $\gamma \propto A^{1/2}$.

3.4. Magnetoresistance

Figure 7 shows the magnetoresistance, $(\rho(B) - \rho(0))/\rho(0)$, as a function of field at various temperatures for $Ce_8Pd_{24}Ga$. At 1.8 K the magnetoresistance is positive and exhibits B^2-dependence up to a field of 12 T. At 12 T, $\Delta\rho/\rho$ reaches a value of 6%. It is generally observed that $\Delta\rho/\rho$ exhibits a positive sign for antiferromagnetic compounds if no superzone gap formation takes place at T_N [28]. For $Ce_8Pd_{24}Ga$ the resistivity does not show any sign of superzone gap formation; hence the observed positive sign of the magnetoresistance is

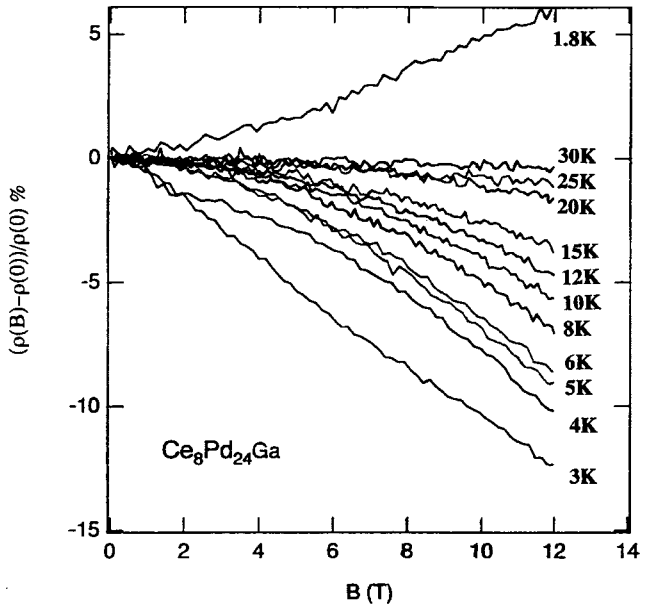

Figure 7. Magnetoresistance, $\Delta\rho/\rho$, as a function of magnetic field at various temperatures for $Ce_8Pd_{24}Ga$.

consistent with the antiferromagnetic ground state. At 3 K the magnetoresistance changes sign from positive to negative and exhibits a linear behaviour with field and eventually reaches a value of -12% at 12 T. Above 3 K the magnitude of the negative magnetoresistance decreases with increasing temperature and becomes almost negligible at 30 K. This type of behaviour of the magnetoresistance is expected for incoherent Kondo scattering of conduction electrons with 4f moments as theoretically proposed by Schlottmann [29]. Schlottmann has calculated the magnetoresistance in the Coqblin–Schrieffer model using the Bethe-*ansatz* technique for various values of the total angular momentum (J) of the Kondo impurity between 1/2 and 5/2. The calculations show a universal behaviour of the magnetoresistance as a function of field and temperature for a given value of J. This indicates that the physics of a single-ion Kondo impurity is governed by a single characteristic energy B^* which is related to the Kondo temperature $T_K = B^*(0)(g\mu/k)$, where the symbols have their usual meaning. Further, it has been observed that $B^*(T)$ varies linearly with temperature, i.e. $B^*(T) = B^*(0) + (k/g\mu)T$ [30]. This shows that T_K can be estimated from the intercept and slope of a B^* versus T plot.

Our inelastic neutron scattering studies revealed that the CF ground state of $Ce_8Pd_{24}Ga$ is a doublet and that the first excited state lies at 3.2 meV, so at low temperatures we can treat each Ce^{3+} ion as an effective $J = 1/2$ spin impurity. Hence we can use Schlottmann's model for $J = 1/2$ to analyse our magnetoresistance at low temperatures. The solid line in figure 8 shows the universal curve of Schlottmann's model for $J = 1/2$. The experimental magnetoresistance data at various temperatures have been scaled to the theoretical curve by adjusting the temperature dependence of $B^*(T)$ at each temperature. The scaling behaviour of the magnetoresistance is apparent from figure 8 between 5 and 30 K. The values of $B^*(T)$ obtained from the analysis are plotted as a function of temperature in the inset of figure 8. The $B^*(T)$ versus T plot exhibits linear behaviour up to 15 K and deviates from linearity above 15 K. This deviation is due to the increase of the population of the first excited crystal-field level with increasing temperature. We have used the low-temperature ($T \leqslant 15$ K) linear behaviour

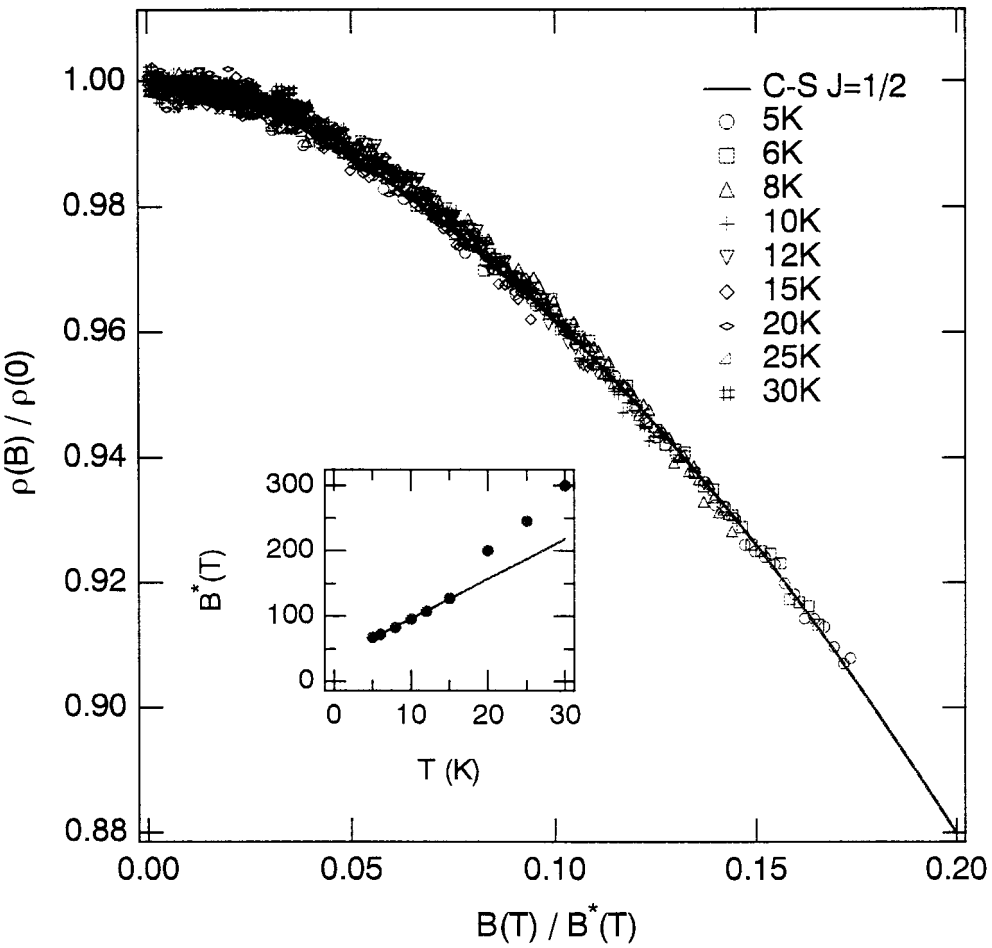

Figure 8. Normalized magnetoresistance, $\rho(B)/\rho(0)$, as a function of B/B^* for $Ce_8Pd_{24}Ga$ at various temperatures. The scaling field B^* has been adjusted at each temperature to minimize the deviation between data points and Schlottmann's theoretical magnetoresistance curve for a $J = 1/2$ Kondo impurity (solid line). The inset shows B^* versus temperature.

of the $B^*(T)$ versus T plot to estimate the value of $T_K = 5.8(\pm 0.3)$ K for $Ce_8Pd_{24}Ga$. This value of $T_K = 5.8$ K is higher than the value 1.6 K estimated from the heat capacity. We have used the extrapolated value of $\gamma_p(T \to 0) = 3.3$ J mol^{-1} K^{-2} from reference [17] to estimate T_K by using the expression $T_K = (N-1)\pi R/6\gamma_p$, where N is the degeneracy of the ground state and R is the gas constant. The low value of T_K estimated from the heat capacity suggests that the calculated value of γ_p may be too high. As mentioned earlier, an artificially high value of γ_p could arise because it has been estimated from measurements in the temperature range between 7 and 16 K where the heat capacity exhibits a Schottky anomaly.

3.5. Magnetic susceptibility

The magnetic susceptibility exhibits Curie–Weiss (CW) behaviour between 20 K and 300 K (figure 9) with an effective paramagnetic moment $\mu_{eff} = 2.33(\pm 0.03)\ \mu_B$ and paramagnetic Curie temperature $\theta_p = -18.8(\pm 0.4)$ K. A small deviation from CW behaviour has been

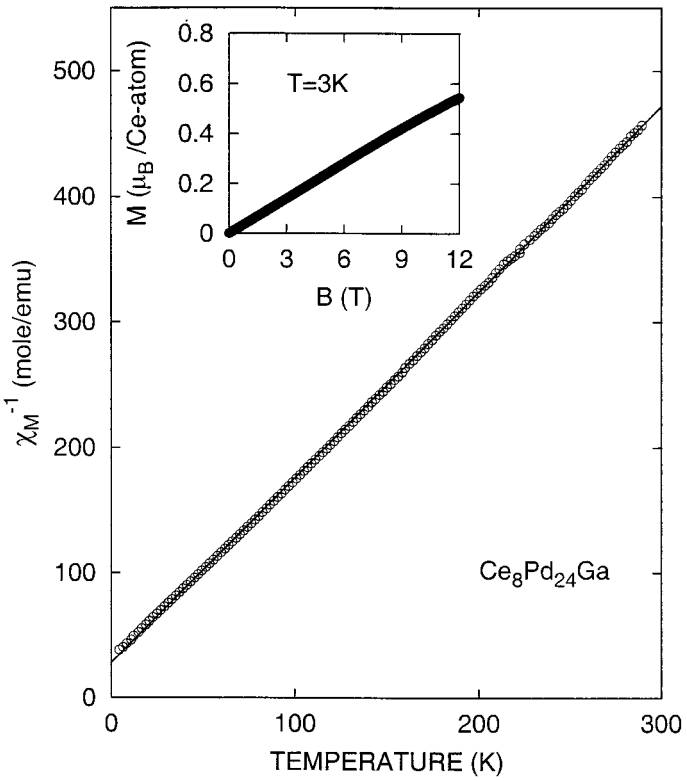

Figure 9. Inverse magnetic susceptibility versus temperature for $Ce_8Pd_{24}Ga$. The inset shows the magnetization isotherm at 3 K for $Ce_8Pd_{24}Ga$.

observed below 20 K, which we attribute to the crystalline-electric-field effect on the $J = 5/2$ multiplet of the Ce^{3+} ion. The observed value of μ_{eff} is slightly smaller than the value 2.54 μ_B of the free Ce^{3+} ion ($J = 5/2$). At present the origin of this is not clear, but it may be attributable to the 22% vacancy on the Ga site. Thus the Ce ions close to this vacant site may have mixed-valence nature as in $CePd_3$. The observed negative sign of θ_p is in agreement with the antiferromagnetic ground state. The magnetization isotherm at 3 K exhibits almost linear behaviour with field up to 12 T with the value of the magnetic moment 0.55 μ_B/Ce atom at 12 T (see the inset of figure 9).

4. Conclusions

The compound $Ce_8Pd_{24}Ga$, which is closely related to the mixed-valence material $CePd_3$, has been investigated using various experimental techniques. Neutron powder diffraction studies show that the compound crystallizes in a new cubic structure with space group $Pm\bar{3}m$. This new cubic structure is composed of distorted perovskite and subcells of Cu_3Au structure arranged with the perovskite-like units centred on the corners of the cube. Inelastic neutron scattering studies show two well defined crystal-field excitations centred at 3.2 meV and 12.8 meV. The analysis of the inelastic neutron scattering data has been performed on the basis of the crystal-field model. The heat capacity calculated using the crystal-field level scheme shows good agreement with the experimental results, and partly explains the reported high value of

the electronic coefficient, γ_p. The resistivity shows the presence of Kondo and crystal-field effects. The low-temperature resistivity (below T_N) reveals the presence of a gap of 16.1 K in the spin-wave spectrum. The critical divergence, near T_N, in $\mathrm{d}\rho/\mathrm{d}T$ is similar to that observed in the heat capacity, which is in agreement with the theory [23]. The magnetoresistance exhibits scaling behaviour in the paramagnetic regime, leading to a Kondo temperature of 5.8 K for $Ce_8Pd_{24}Ga$. The magnetic susceptibility exhibits Curie–Weiss behaviour between 20 K and 300 K with an effective paramagnetic moment $\mu_{eff} = 2.33\ \mu_B$.

The chemical formula of the compound $Ce_8Pd_{24}Ga$ can also be written as $CePd_3Ga_{0.125}$ in order to make direct comparison with $CePd_3$. This reveals that the transport and magnetic properties of $CePd_3$ change strongly with incorporation of the Ga atom in the cubic cell. These changes in the properties could be attributed to the dehybridization of Ce 4f and Pd 4d electrons as a result of the shorter bond length between Pd2 and Ga atoms in $Ce_8Pd_{24}Ga$. The shorter Pd2–Ga bond length could produce a strong overlap between the p electrons of the Ga and d electrons of the Pd and hence dehybridization between Ce 4f and Pd 4d electrons.

References

[1] Goremychkin E A, Osborn R and Sashin I L 1999 *J. Appl. Phys.* **85** (pt2B) 6046
[2] Wasylecko L O, Grin Y N and Fedorchuk A A 1995 *J. Alloys Compounds* **219** 222
[3] Gardner W E, Penfold J, Smith T F and Harris I R 1972 *J. Phys. F: Met. Phys.* **2** 133
Kappler J P, Besnus M J, Lehmann P and Meyer A 1985 *J. Less-Common Met.* **111** 261
[4] Ikeda K and Gschneidner K A Jr 1982 *Phys. Rev.* B **25** 4623
[5] Scoboria P, Crow J E and Mihalisin T 1979 *J. Appl. Phys.* **50** 1895
[6] Furrer A and Purwins H G 1976 *J. Phys. C: Solid State Phys.* **9** 1491
Loewenhaupt M and Holland-Moritz E 1979 *J. Appl. Phys.* **50** 7456
[7] Jaccard D and Sierro J 1982 *Valence Instabilities* ed P Wachter and H Boppart (Amsterdam: North-Holland) p 409
[8] Webb B C, Sievers A J and Mihalisin T 1986 *Phys. Rev. Lett.* **57** 1951
[9] Doniach S 1997 *Valence Instabilities and Related Narrow-Band Phenomena* ed R D Parks (New York: Plenum) p 169
Doniach S 1977 *Physica* B **91** 231
[10] Takahashi H, Takegahara K, Yanase A and Kasuya T 1982 *Valence Instabilities* ed P Wachter and H Boppart (Amsterdam: North-Holland) p 379
Kasuya T 1985 *Theory of Heavy Fermions and Valence Fluctuations* ed T Kasuya and T Saso (Berlin: Springer) p 2
[11] Dhar S K, Malik S K and Vijayaraghavan R 1981 *Phys. Rev.* B **24** 8182
Kappler J P, Besnus M J, Beaurepaire E, Meyer A, Sereni J and Nieva G 1985 *J. Magn. Magn. Mater.* **47+48** 111
Sereni J 1991 *Handbook on the Physics and Chemistry of Rare Earths* vol 15, ed K A Gschneidner Jr and L Eyring (Amsterdam: North-Holland) p 1
[12] Culverhouse S R, Rainford B D and Paul D M^{c}K 1992 *J. Magn. Magn. Mater.* **108** 121
[13] Houshiar M, Adroja D T and Rainford B D 1996 *Physica* B **223+244** 268
[14] Adroja D T, Rainford B D and Jansen A G M 1996 *J. Magn. Magn. Mater.* **140–144** 1217
[15] Gordon R A and DiSalvo F J 1996 *Z. Naturf.* b **51** 52
[16] Gordon R A, Jones C D W, Alexander M G and DiSalvo F J 1996 *Physica* B **225** 23
[17] Cho B K, Gordon R A, Jones C D W and DiSalvo F J 1998 *Phys. Rev.* B **57** 15 191
[18] Ibberson R M 1993 Profile analysis of neutron powder diffraction data *Rutherford Appleton Laboratory Report* RAL-92-032, Version 2.2
[19] Murani A P 1994 *Phys. Rev.* B **50** 9882
[20] Houshiar M 1997 *PhD Thesis* Southampton University, UK
Rainford B D, Adroja D T and Houshiar M 2001 to be published
[21] Newman D J 1971 *Adv. Phys.* **20** 197
Newman D J and Ng B 1989 *Rep. Prog. Phys.* **52** 699
[22] Stevens K W H 1952 *Proc. Phys. Soc.* A **65** 209
[23] Kasuya T and Kondo A 1974 *Solid State Commun.* **14** 249

Kasuya T and Kondo A 1974 *Solid State Commun.* **14** 253
[24] Cornut B and Coqblin B 1972 *Phys. Rev.* B **5** 4541
[25] Fischer K H 1989 *Z. Phys.* B **74** 475
Fischer K H 1989 *Z. Phys.* B **76** 315
[26] Anderson N H 1980 *Crystalline Field and Structural Effects in f-Electron Systems* ed J E Crow, R P Guertin and T W Mihalisin (New York: Plenum) p 373
[27] Thompson J D and Lawrence J M 1994 *Handbook on the Physics and Chemistry of Rare Earths* vol 19, ed K A Gschneidner Jr, L Eyring, G H Lander and G R Choppin (Amsterdam: North-Holland) p 383
[28] Guzik A and Pierre J 1998 *J. Alloys Compounds* **264** 8
Lakshmi K V, Menon L, Nigam A K, Das A and Malik S K 1996 *Physica* B **224** 289
Yamada H and Takada S 1973 *J. Phys. Soc. Japan* **34** 51
[29] Schlottmann P 1983 *Z. Phys.* B **51** 223
[30] Adroja D T, Rainford B D and Neville A J 1996 *Physica* B **223+224** 279
Bauer E 1984 *Adv. Phys.* **40** 373